Archival Report

Biological Psychiatry: Celebrating 50 Years

Chronic Stress Remodels Synapses in an Amygdala Circuit–Specific Manner

Jun-Yu Zhang, Tao-Hui Liu, Ye He, Han-Qing Pan, Wen-Hua Zhang, Xiao-Ping Yin, Xiao-Li Tian, Bao-Ming Li, Xiao-Dong Wang, Andrew Holmes, Ti-Fei Yuan, and Bing-Xing Pan

ABSTRACT

BACKGROUND: Chronic stress exposure increases the risk of developing various neuropsychiatric illnesses. The behavioral sequelae of stress correlate with dendritic hypertrophy and glutamate-related synaptic remodeling at basolateral amygdala projection neurons (BLA PNs). Yet, though BLA PNs are functionally heterogeneous with diverse corticolimbic targets, it remains unclear whether stress differentially impacts specific output circuits.

METHODS: Confocal imaging was used to reconstruct the morphology of mouse BLA PNs with the aid of retrograde tracing and biocytin staining. The synaptic activity in these neurons was measured with in vitro electrophysiology, and anxiety-like behavior of the mice was assessed with the elevated plus maze and open field test.

RESULTS: Chronic restraint stress (CRS) produced dendritic hypertrophy across mouse BLA PNs, regardless of whether they did (BLA→dorsomedial prefrontal cortex [dmPFC]) or did not (BLA↛dmPFC) target dmPFC. However, CRS increased the size of dendritic spine heads and the number of mature, mushroom-shaped spines only in BLA↛dmPFC PNs, sparing neighboring BLA→dmPFC PNs. Moreover, the excitatory glutamatergic transmission was also selectively increased in BLA↛dmPFC PNs, and this effect correlated with CRS-induced increases in anxiety-like behavior. Segregating BLA↛dmPFC PNs based on their targeting of ventral hippocampus (BLA→ventral hippocampus) or nucleus accumbens (BLA→nucleus accumbens) revealed that CRS increased spine density and glutamatergic signaling in BLA→ventral hippocampus PNs in a manner that correlated with anxiety-like behavior.

CONCLUSIONS: Chronic stress caused BLA PN neuronal remodeling with a previously unrecognized degree of circuit specificity, offering new insight into the pathophysiological basis of depression, anxiety disorders, and other stress-related conditions.

Keywords: Amygdala, Anxiety, Prefrontal cortex, Projection neuron, Spine, Stress

https://doi.org/10.1016/j.biopsych.2018.06.019

Maladaptive responses to prolonged stress are associated with the onset and exacerbation of neuropsychiatric diseases, including mood and anxiety disorders (1–4). Heightened activity within the amygdala, a brain region essential for the regulation of fear and anxiety, has been implicated in stress-related emotional abnormalities in humans and animal models (5–8). Moreover, the amygdala exhibits profound functional changes as a result of chronic stress that are closely linked to attendant changes in anxiety (5,6,9–12). For instance, in contrast to the stress-induced dendritic retraction seen in other nodes within the corticolimbic system, such as the dorsomedial prefrontal cortex (dmPFC) and hippocampus (13), projection neurons (PNs) within the basolateral amygdala (BLA) display lasting dendritic hypertrophy after chronic stress (9,14,15) but dendritic retraction after acute stress (11).

The BLA is connected through PNs to the dmPFC, ventral hippocampus (vHPC), and various other regions involved in higher-order behavioral processes, including the nucleus accumbens (NAc) (16). Notably, there appears to be relatively little collateralization of BLA PNs to these target regions (17), suggesting a high degree of projection specificity. However, within the BLA there is no clear spatial organization of PNs based on their primary output target, and it is only recently, with the advent of new techniques for functional circuit mapping, that the role of specific BLA output pathways has begun to be delineated (17–21). This work has, for instance, proposed that BLA PNs innervating the NAc and vHPC primarily encode information with positive and negative valence, respectively (17,20,22,23).

Despite emerging evidence of the functional and anatomical heterogeneity of BLA output pathways, it remains unclear whether the effects of stress are restricted to specific output circuits or manifest more ubiquitously across BLA neurons. We addressed this question by labeling mouse BLA PNs using fluorescent RetroBeads IX to differentiate BLA PNs targeting the dmPFC (BLA→dmPFC) from those not targeting the dmPFC (BLA↛dmPFC) and then examining each population for chronic restraint stress (CRS)–induced changes in dendritic morphology, spine density and morphology, and excitatory glutamatergic synaptic transmission.

We found that CRS amplified excitatory transmission and increased spine density and the number of mature, mushroom-

SEE COMMENTARY ON PAGE e7

ISSN: 0006-3223

shaped spines in BLA↛dmPFC, but not BLA→dmPFC, PNs. Based on this finding, we then segregated BLA↛dmPFC PNs into subpopulations of BLA PNs targeting vHPC (BLA→vHPC) and targeting NAc (BLA→NAc) and found that only BLA→vHPC PNs showed spine proliferation and increased glutamatergic transmission after CRS. Additionally, we found that the CRS-induced increases in excitatory transmission in BLA→vHPC PNs correlated with heightened anxiety-like behavior. Collectively, our findings revealed a previously unidentified degree of specificity in the effects of chronic stress on discrete functional BLA circuits.

METHODS AND MATERIALS

Animals

Male C57BL/6 mice were used and housed in groups (3–5 per cage) in a temperature- and humidity-controlled animal facility with ad libitum access to food and water under a 12-hour light/dark cycle. Mice were raised under the care of the Division of Laboratory Animals, Nanchang University. All experimental procedures were approved by the Institutional Animal Care and Use Committee of Nanchang University.

Chronic Restraint Stress

At 50 to 53 days of age, mice were subjected to CRS by placing them in a restraint cylinder fitted closely to body size and drilled with holes to allow free breathing for 1 session per day at around 2 PM, for 2 hours per session, for 10 consecutive days. Mice assigned to acute stress experienced only 1 session of 2-hour restraint stress. The control mice were transferred in their home cages to the experimental room at 2 PM, gently handled for 2 to 4 minutes, and returned back to the holding room about 2 hours later for 10 consecutive days.

Electrophysiological Recordings

Electrophysiological recordings were performed as we described previously (24). More detailed information appears in the Supplement.

Stereotaxic RetroBead Injections

RetroBeads (Lumafluor, Inc., Durham, NC) were injected 7 to 10 days before stress (mice aged 40–43 postnatal days) via stereotaxic surgery under general anesthesia of 2% pentobarbital sodium (4.5 mL/kg) using a stereotaxic instrument (Stoelting Co., Wood Dale, IL). RetroBeads (0.5 μL per side) were injected into the dmPFC, vHPC, and NAc at the following stereotaxic coordinates: dmPFC, 1.94 mm rostral to bregma, ±0.35 mm lateral to midline, and 2.5 mm ventral to bregma; vHPC, −3.6 mm rostral to bregma, ±3.3 mm lateral to midline, and 3.7 mm ventral to bregma; NAc, 1.42 mm rostral to bregma, ±0.85 mm lateral to midline, and 4.7 mm ventral to bregma. Injections were performed using glass micropipettes with their tip diameters of approximately 10 to 20 μm (pulled with PC-10 Puller [Narishige Co., Ltd., Tokyo, Japan]). After injection, the pipette was left in the injection site for an additional 5 minutes before being pulling out slowly. The mice were moved to their home cages after full recovery from anesthesia. To control the reproducibility of the RetroBead injection across mice, we included for analysis only mice with amygdala sections (70-μm thickness) containing >250 RetroBead-labeled cells/mm^2.

Biocytin Filling and Neuronal Reconstruction

Coronal sections 340 μm thick containing the amygdala were examined for individual PNs with distinct projection targets, which were then recorded using patch clamp under whole-cell configuration. The pipette tip was filled with biocytin-free medium by gentle suction, followed by backfilling the pipette with 0.5% biocytin (Life Technologies Corp., Carlsbad, CA) dissolved in the patch solution. Only neurons that maintained stable membrane potential for at least 20 minutes were included. On cessation of filling, the pipette was slowly pulled out along the direction of recording until a membrane reseal was formed. After a 10-minute recovery, the slices were fixed in 4% paraformaldehyde overnight, cryoprotected in 30% sucrose solution, and incubated with avidin Alexa Fluor 488 (Life Technologies Corp.) conjugate in phosphate-buffered saline containing Triton X-100 (Sigma-Aldrich, St. Louis, MO) overnight at 4°C.

Sections were coverslipped with Vectashield aqueous mounting medium (Vector Laboratories, Inc., Burlingame, CA), and the individual biocytin-labeled PNs were traced with an Olympus FV1000 confocal microscope (Olympus Corp., Tokyo, Japan) at 400× magnification and reconstructed using Neurolucida software (MBF Bioscience, Williston, VT). PNs were included for analysis only when their dendritic trees were

Figure 1. Chronic restraint stress (CRS) causes dendritic hypertrophy in basolateral amygdala (BLA) projection neurons (PNs) targeting dorsomedial prefrontal cortex (dmPFC) (BLA→dmPFC) and not targeting dmPFC (BLA↛dmPFC). **(A)** Schematic showing injection of red fluorescent RetroBeads into dmPFC to label BLA→dmPFC PNs in the BLA. **(B)** Examples of RetroBead-labeled BLA→dmPFC and BLA↛dmPFC PNs filled with biocytin using patch clamp recording under whole-cell configuration (scale bar = 10 μm). **(C)** Examples of reconstructed BLA→dmPFC PNs from unstressed control mice and CRS-exposed mice (scale bar = 30 μm). **(D)** Sholl analysis of dendritic length as a function of distance from the soma in BLA→dmPFC PNs. Averaged total dendritic length (inset). Distance × CRS two-way analysis of variance (ANOVA): interaction ($F_{9,152}$ = 1.77, p = .079), main effect of distance ($F_{9,152}$ = 45.14, p < .001), main effect of CRS ($F_{1,152}$ = 13.60, p < .001). *t* test: *p < .05, **p < .01, n = 9 neurons/5 control mice, n = 12 neurons/6 CRS-exposed mice. **(E)** Average dendritic branch number in BLA→dmPFC PNs. *t* test: **p < .01. **(F)** Examples of reconstructed BLA↛dmPFC PNs from unstressed control mice and CRS-exposed mice (scale bar = 30 μm). **(G)** Sholl analysis of dendritic length as a function of its distance from the soma in BLA↛dmPFC PNs. Averaged total dendritic length (inset). Distance × CRS two-way ANOVA: interaction ($F_{8,99}$ = 0.803, p = .602), main effect of distance ($F_{8,99}$ = 36.91, p < .001), main effect of CRS ($F_{1,99}$ = 9.65, p = .003). *t* test: *p < .05, **p < .01, n = 8 neurons/5 control mice, n = 8 neurons/5 CRS-exposed mice. **(H)** Average dendritic branch number in BLA↛dmPFC PNs. *t* test: **p < .01. **(I, J)** Average branch number in proximal and distal dendrites of BLA→dmPFC **(I)** and BLA↛dmPFC **(J)** PNs. For BLA→dmPFC PNs, distance × CRS two-way ANOVA: interaction ($F_{1,36}$ = 0.426, p = .518), main effect of distance ($F_{1,36}$ = 11.66, p = .002), main effect of CRS ($F_{1,36}$ = 12.21, p = .001). *t* test: *p < .05. For BLA↛dmPFC PNs, distance × CRS two-way ANOVA: interaction ($F_{1,24}$ = 1.52, p = .229), main effect of distance ($F_{1,24}$ = 2.37, p = .137), main effect of CRS ($F_{1,24}$ = 10.44, p = .004). *t* test: *p < .05. Data are means ± SEM.

completely filled as evidenced by well-defined ending with no visible terminals on the furthest margins. Sholl analysis, total dendrite length, and branching number were determined using NeuroExplorer software (MBF Bioscience, Williston, VT). Neurons were traced by an independent experimenter blinded to the group. Owing to the stellate appearance of many of the

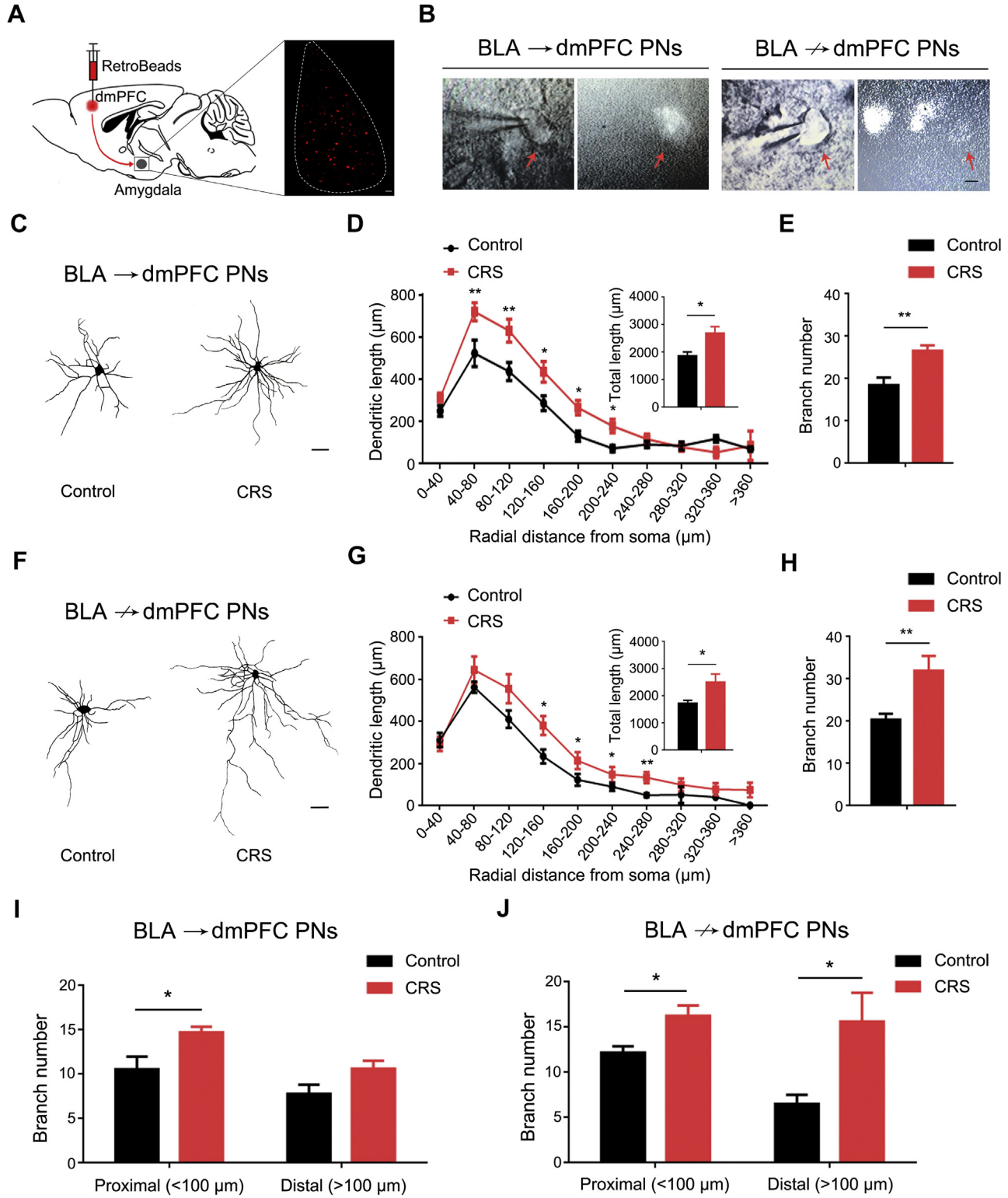

BLA neurons, we did not distinguish the apical versus basal dendrites (25,26).

To reconstruct the dendritic spines, the coronal sections were resectioned at 70 μm and analyzed with the FV1000 confocal microscope. The images were taken using the UPLSAPO 100× oil-immersion lens (Olympus Corp.) (numerical aperture of 1.40). We used 1024 × 1024 pixels for frame size without zooming. Serial stack images with step size ranging from 0.3 to 0.5 μm were collected. The dendritic spines were reconstructed using Neurolucida software. Dendrites located at least 20 μm away from the soma and longer than 15 μm were randomly selected for analysis of spine density and head size. For individual cells, 8 to 12 dendritic segments were selected. Dendritic spines were counted and categorized with the aid of ImageJ software (National Institute of Mental Health, Bethesda, MD) (27). Spines were classified into three subtypes—thin, mushroom, and stubby—based on previously described criteria, with minor modifications (28). Briefly, thin spines included a head-to-neck diameter ratio less than 1.1 and a length-to-spine head diameter greater than 2.0. Mushroom spines had a head diameter larger than 0.5 μm and a head-to-neck diameter ratio greater than 1.1. Stubby spines had no clear border between the head and the attachment to the shaft. To calculate the mean spine head size in different PN populations across groups, all spines from the given population were pooled.

Anxiety-like Behavior

The anxiety-like behavior of mice was tested with the elevated plus maze and open field test as previously described (29) with minor modifications. For the elevated plus maze (Med Associates, Inc., St. Albans, VT), the mouse was placed in the center of the maze facing one of the two closed arms for a 10-minute test. The number of entries and time spent in the open arms was measured with video tracking software (DOC-086; Med Associates, Inc.). The open field was a square chamber (50 × 50 cm), and a 25 × 25 cm center square was color marked. Mice were placed in the center and monitored for 10 minutes with an overhead video tracking system that recorded the animal's location and path and the time the animal spent in the center square.

Statistics

Data are represented as mean ± SEM. Unless otherwise stated, the neuronal morphometry and miniature excitatory postsynaptic current (mEPSC) parameters were analyzed with two-way analysis of variance with the neuronal population as a within-subjects factor and group (stressed or control) as a between-subjects factor. Post hoc comparisons were made using Bonferroni-corrected *t* test. Two-tailed *t* test was used to compare the morphometry of the randomly selected BLA PNs between stressed and nonstressed mice. Significance levels were set at $p < .05$. Spine head diameters and the decay of *N*-methyl-D-aspartate receptor currents were analyzed by Kolmogorov-Smirnov comparison, and $p < .001$ was set as the threshold for significance because of high degree of statistical power in these data. The homoscedasticity and normality of the distributions were analyzed with Bartlett's test and Kolmogorov-Smirnov test, respectively. Statistical analyses were performed using Graphpad Prism Version 5 (GraphPad Software, La Jolla, CA).

RESULTS

CRS Causes Generalized Dendritic Hypertrophy in BLA PNs

We first assessed the impact of CRS on dendritic morphology in BLA PNs, regardless of their projection targets. Consistent with previous studies showing that CRS causes dendritic hypertrophy in amygdala PNs of rats (14), we found that C57BL/6J mice subjected to CRS exhibited significantly increased dendritic length and branch number compared with nonstressed control mice (Supplemental Figure S1A–C). Sholl analysis showed that increased dendritic length was particularly prominent in dendrites proximal to the soma, whereas increased branch number was evident both proximally and distally (Supplemental Figure S1D, E).

We then asked whether CRS-induced dendritic changes differed as a function of the target of the BLA PNs by examining morphology in BLA→dmPFC and BLA↛dmPFC PNs. This was achieved by injecting red fluorescent RetroBeads into the dmPFC and then biocytin-staining fluorescent (BLA→dmPFC) and nonfluorescent (putative BLA↛dmPFC) PNs in the BLA with the aid of whole-cell patch recording (Figure 1A, B). For both PN populations, CRS significantly increased dendritic length and branch number in both PN populations, relative to unstressed control mice (Figure 1C–H). There was a difference in the spatial distribution pattern of hypertrophy, with increased dendritic length unbiased toward both the soma/proximal and distal regions in BLA→dmPFC PNs (Figure 1D) but only in the distal areas in BLA↛dmPFC PNs (Figure 1G). However, the branch number proliferation emerged only in the soma/proximal regions of BLA→dmPFC PNs (Figure 1I) but both proximally and distally to the soma of BLA↛dmPFC cells (Figure 1J). The main finding from these morphologic analyses is that, replicating prior data, CRS produces robust dendritic hypertrophy in BLA PNs and that these effects are generalized regardless of whether the PNs target the dmPFC.

CRS Selectively Remodels Dendritic Spines in BLA↛dmPFC PNs

We next assessed the effects of CRS at the level of dendritic spines in BLA PNs. When PNs were considered as a whole, i.e., regardless of dmPFC targeting, we observed a nonsignificant trend for increased spine density and a significant increase in spine head diameter after CRS (Supplemental Figure S2A–C). When segregated into BLA→dmPFC and BLA↛dmPFC PNs, the effects of CRS on spine density were again mild (Figure 2A, B), but the CRS-induced increase in spine head diameter was found to be restricted to BLA↛dmPFC PNs, with no effect on neighboring BLA→dmPFC cells (Figure 2C, D).

To gain more insight into the changes in dendritic spines produced by CRS, we separately analyzed spines based on the classic categorizations of thin, stubby (both considered to represent immature spines), and mushroom (mature) in their morphology (30). Consistent with the increase in head

diameter in BLA↛dmPFC PNs, CRS was associated with a significantly higher density of mushroom, but not thin or stubby, spines, whereas no change was evident in BLA→dmPFC PNs for any spine type (Figure 2E, F). Within each subcategory of spine type, head size was unaltered by CRS in either PN population (Supplemental Figure S3). These data show that the generalized dendritic hypertrophy produced by CRS is associated with a preponderance of mature mushroom spines that is restricted to BLA PNs that do not target the dmPFC.

CRS Augments Excitatory Transmission in BLA↛dmPFC PNs

The dendritic spine is the postsynaptic component of glutamatergic signaling and a critical locus for synaptic plasticity (31,32). The increased mature mushroom spines in

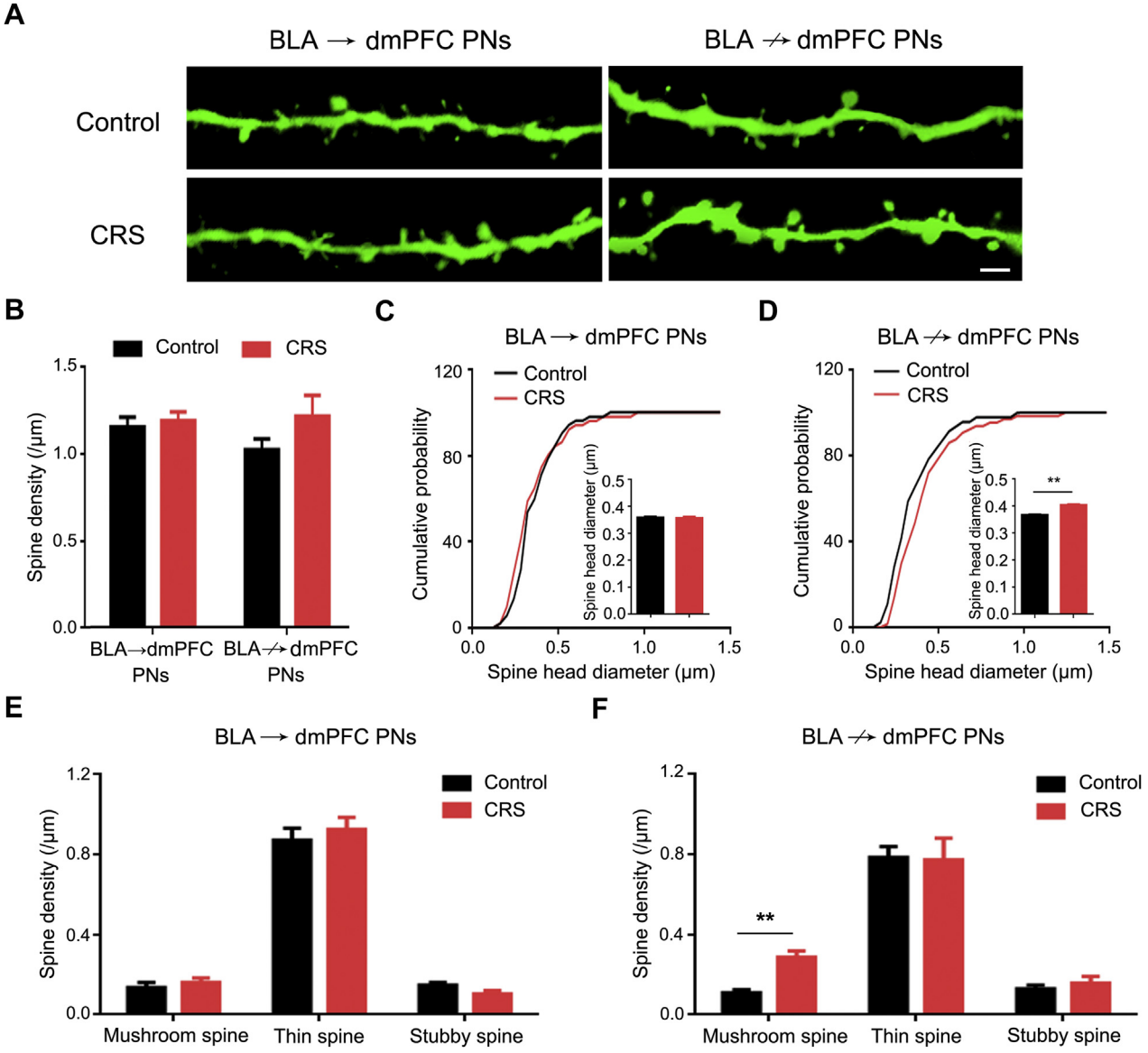

Figure 2. Chronic restraint stress (CRS) remodels dendritic spines in basolateral amygdala (BLA) projection neurons (PNs) not targeting dorsomedial prefrontal cortex (dmPFC) (BLA↛dmPFC) but not BLA PNs targeting dmPFC (BLA→dmPFC). **(A)** Representative images of dendritic spines in BLA→dmPFC and BLA↛dmPFC PNs from unstressed control mice and CRS-exposed mice (scale bar = 2 μm). **(B)** Average spine density in BLA→dmPFC and BLA↛dmPFC PNs. PN group × CRS two-way analysis of variance: interaction ($F_{1,31}$ = 1.21, p = .281), main effect of PN group ($F_{1,31}$ = 0.54, p = .466), main effect of CRS ($F_{1,31}$ = 2.53, p = .122). For BLA→dmPFC PNs, n = 9 neurons/8 control mice, n = 9 neurons/8 CRS-exposed mice. For BLA↛dmPFC PNs, n = 10 neurons/9 control mice, n = 7 neurons/7 CRS-exposed mice. **(C)** Cumulative probability of spine head diameter in BLA→dmPFC PNs. Control mice, n = 4108 spines/9 neurons; CRS-exposed mice, n = 4240 spines/9 neurons. Kolmogorov-Smirnov test: p = .956. Inset shows the average spine head diameter. t test: p = .123. **(D)** Cumulative probability of spine head diameter in BLA↛dmPFC PNs. Control mice, n = 5348 spines/10 neurons; CRS-exposed mice, n = 3459 spines/7 neurons. Kolmogorov-Smirnov test: $p < .001$. Inset shows the average spine head diameter. t test: $^{**}p < .01$. **(E, F)** Average density in mushroom, thin, and stubby spines in BLA→dmPFC **(E)** and BLA↛dmPFC **(F)** PNs. t test: $^{**}p < .01$. Data are means ± SEM.

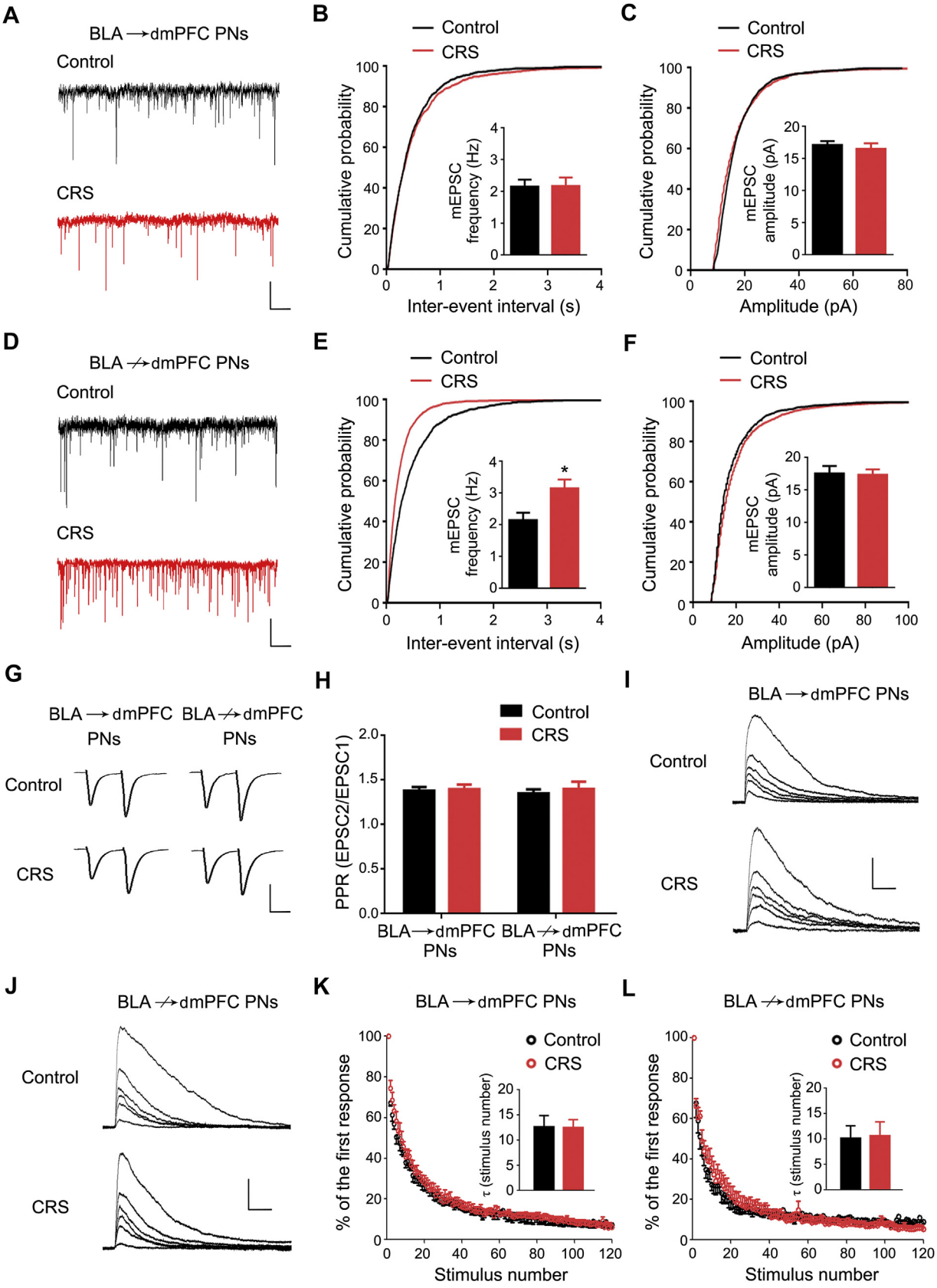
A
BLA → dmPFC PNs
Control
CRS
B
Control
CRS
Cumulative probability
mEPSC frequency (Hz)
Inter-event interval (s)
C
Control
CRS
Cumulative probability
mEPSC amplitude (pA)
Amplitude (pA)
D
BLA ⇢ dmPFC PNs
Control
CRS
E
Control
CRS
Cumulative probability
mEPSC frequency (Hz)
*
Inter-event interval (s)
F
Control
CRS
Cumulative probability
mEPSC amplitude (pA)
Amplitude (pA)
G
BLA → dmPFC PNs
BLA ⇢ dmPFC PNs
Control
CRS
H
Control
CRS
PPR (EPSC2/EPSC1)
BLA → dmPFC PNs
BLA ⇢ dmPFC PNs
I
BLA → dmPFC PNs
Control
CRS
J
BLA ⇢ dmPFC PNs
Control
CRS
K
BLA → dmPFC PNs
Control
CRS
% of the first response
τ (stimulus number)
Stimulus number
L
BLA ⇢ dmPFC PNs
Control
CRS
% of the first response
τ (stimulus number)
Stimulus number

BLA↛dmPFC, but not BLA→dmPFC, PNs therefore led us to examine whether CRS differentially affected glutamatergic transmission onto these two neuronal populations. To test for this, we recorded postsynaptic mEPSCs at PNs in the presence of tetrodotoxin (1 μmol/L) (Fisheries Research Institute, Hebei Province, China) and picrotoxin (100 μmol/L) (Sigma-Aldrich) to block action potentials and gamma-aminobutyric acid A receptor currents, respectively. Although neither the frequency nor amplitude of mEPSCs in BLA→dmPFC PNs differed between CRS-exposed mice and unstressed control mice (Figure 3A–C), CRS produced significantly higher mEPSC frequency in BLA↛dmPFC PNs, with no effect on amplitude (Figure 3D–F).

An increase of mEPSC frequency in BLA↛dmPFC, but not BLA→dmPFC, PNs after CRS is in accordance with the selective increase in mushroom spine density in the former. Alternatively, if CRS increased the presynaptic glutamate release onto BLA↛dmPFC PNs, this could account for the enhanced excitatory transmission we observed in the cells after CRS. To test this possibility, we recorded the evoked EPSCs on two consecutive electrical stimuli (separated by 50 ms) delivered through a bipolar stimulation electrode placed close to the recorded PN (approximately 200 μm), with 100 μmol/L picrotoxin added to the perfusion solution. The paired pulse ratio was calculated as the ratio of the second evoked EPSC amplitude to the first evoked EPSC amplitude as an index of transmitter release probability. We observed paired pulse facilitation that was comparable across CRS condition and PN targeting population (Figure 3G, H).

Next, we examined presynaptic glutamate release probability by measuring the decay of evoked *N*-methyl-D-aspartate receptor–mediated currents in the presence of its noncompetitive antagonist MK-801 (Sigma-Aldrich). For both PN populations, the decay of the current was indistinguishable between CRS-exposed mice and control mice, as demonstrated by similar τ values (Figure 3I–L). Thus, CRS had a negligible influence on presynaptic glutamate release, supporting the notion that the preferential increase in mEPSC frequency in BLA↛dmPFC PNs likely reflects the corresponding increase in mature spine density produced by CRS. These electrophysiological data demonstrate that remodeling of BLA↛dmPFC PNs after CRS is associated with increased glutamatergic transmission onto this population.

CRS-Induced Increase of Glutamatergic Transmission Onto BLA↛dmPFC PNs Correlates With Anxiety-like Behavior

Prior studies have linked the effects of CRS on BLA neuronal function to alterations in fear-, anxiety-, and depression-related behaviors (33–37). Given our finding that CRS selectively enhances glutamatergic transmission and remodels dendritic spines at BLA↛dmPFC PNs, we therefore next examined whether these CRS-induced effects were associated with changes in anxiety-like behavior (Figure 4A).

Mice subjected to CRS exhibited heightened anxiety-like behavior, as indicated by decreased open arm time and entries in the elevated plus maze and less time in the center square in the open field test relative to unstressed control mice (Figure 4B, C). Mice were sacrificed 6 hours after testing to record mEPSCs in RetroBead-labeled BLA→dmPFC and nonlabeled putative BLA↛dmPFC PNs. In unstressed control mice, mEPSC frequency did not correlate with explorations in open arm (elevated plus maze) and center square (open field test) in either population (Figure 4D, F). However, in CRS-exposed mice, the open arm and center square explorations were significantly and inversely correlated with mEPSC frequency (not amplitude) in BLA↛dmPFC, but not BLA→dmPFC, PNs (Figure 4E, G and Supplemental Figure S4). These data show that heightened anxiety-like behavior resulting from CRS is closely associated with increases in glutamatergic transmission onto BLA↛dmPFC PNs.

CRS Affects BLA→vHPC, but Not BLA→NAc, PNs

Thus far, our findings indicate the anxiety-related effects of CRS are linked to changes in neuronal function in BLA PNs that do not target the dmPFC but do not yet address whether these cells target any non-dmPFC region in particular. The vHPC represents one obvious candidate for these effects given prior evidence implicating this region in anxiety-related behavior (38). Moreover, BLA PNs projecting to the vHPC or NAc have been shown to sparsely innervate the dmPFC (17).

We labeled BLA→vHPC PNs using RetroBeads and differentiated these cells from BLA→NAc PNs, finding that the two cells in the two populations were spatially interspersed in a salt-and-pepper manner, with minimal (approximately 7%)

Figure 3. Chronic restraint stress (CRS) increases excitatory transmission in basolateral amygdala (BLA) projection neurons (PNs) not targeting dorsomedial prefrontal cortex (BLA↛dmPFC). **(A)** Representative traces showing miniature excitatory postsynaptic currents (mEPSCs) in BLA PNs targeting dmPFC (BLA→dmPFC) (scale bar = 1 second, 10 pA). **(B, C)** Cumulative probability of the interevent interval **(B)** and amplitude **(C)** of mEPSCs in BLA→dmPFC PNs. Average mEPSC frequency and amplitude (inset). n = 10 neurons/5 control mice, n = 10 neurons/5 CRS-exposed mice. Kolmogorov-Smirnov test for EPSC frequency: $p = .207$. Kolmogorov-Smirnov test for EPSC amplitude: $p = .759$. **(D)** Representative traces showing mEPSCs in BLA↛dmPFC PNs (scale bar = 1 s, 10 pA). **(E, F)** Cumulative probability of the interevent interval **(E)** and amplitude **(F)** of mEPSCs in BLA→dmPFC PNs. Average mEPSC frequency and amplitude (inset). n = 10 neurons/5 control mice, n = 10 neurons/5 CRS-exposed mice. Kolmogorov-Smirnov test for EPSC frequency: $p < .001$. Kolmogorov-Smirnov test for EPSC amplitude: $p = .362$. t test: $^*p < .05$. **(G)** Representative traces showing electrically evoked EPSCs in BLA→dmPFC and BLA↛dmPFC PNs (2 stimuli separated by 50 ms) (scale bar = 20 ms, 150 pA). **(H)** Average paired pulse ratio (PPR) in BLA→dmPFC and BLA↛dmPFC PNs. PN group × CRS two-way analysis of variance: interaction ($F_{1,47} = 0.10$, $p = .755$), main effect of PN group ($F_{1,47} = 0.07$, $p = .796$), main effect of CRS ($F_{1,47} = 0.36$, $p = .550$). For BLA→dmPFC PNs, n = 12 neurons/5 control mice, n = 13 neurons/5 CRS-exposed mice. For BLA↛dmPFC PNs, n = 12 neurons/5 control mice, n = 14 neurons/5 CRS-exposed mice. **(I, J)** Representative traces showing *N*-methyl-D-aspartate receptor–mediated currents in BLA→dmPFC **(I)** and BLA↛dmPFC **(J)** PNs during their progressive blockage by repetitive electric stimuli in the presence of MK-801. The first, fifth, 10th, 20th, 40th, and 80th current traces shown sequentially from top to bottom (scale bar = 200 ms, 150 pA). **(K, L)** *N*-methyl-D-aspartate receptor–mediated current amplitude in the presence of MK-801 as a function of stimulus number (first current amplitude set to 100%). Average tau values (inset). For BLA→dmPFC PNs, n = 8 neurons/4 control mice, n = 7 neurons/4 CRS-exposed mice. t test: $p = .955$. For BLA↛dmPFC PNs, n = 7 neurons/4 control mice, n = 7 neurons/5 CRS-exposed mice. t test: $p = .899$. Data are means ± SEM.

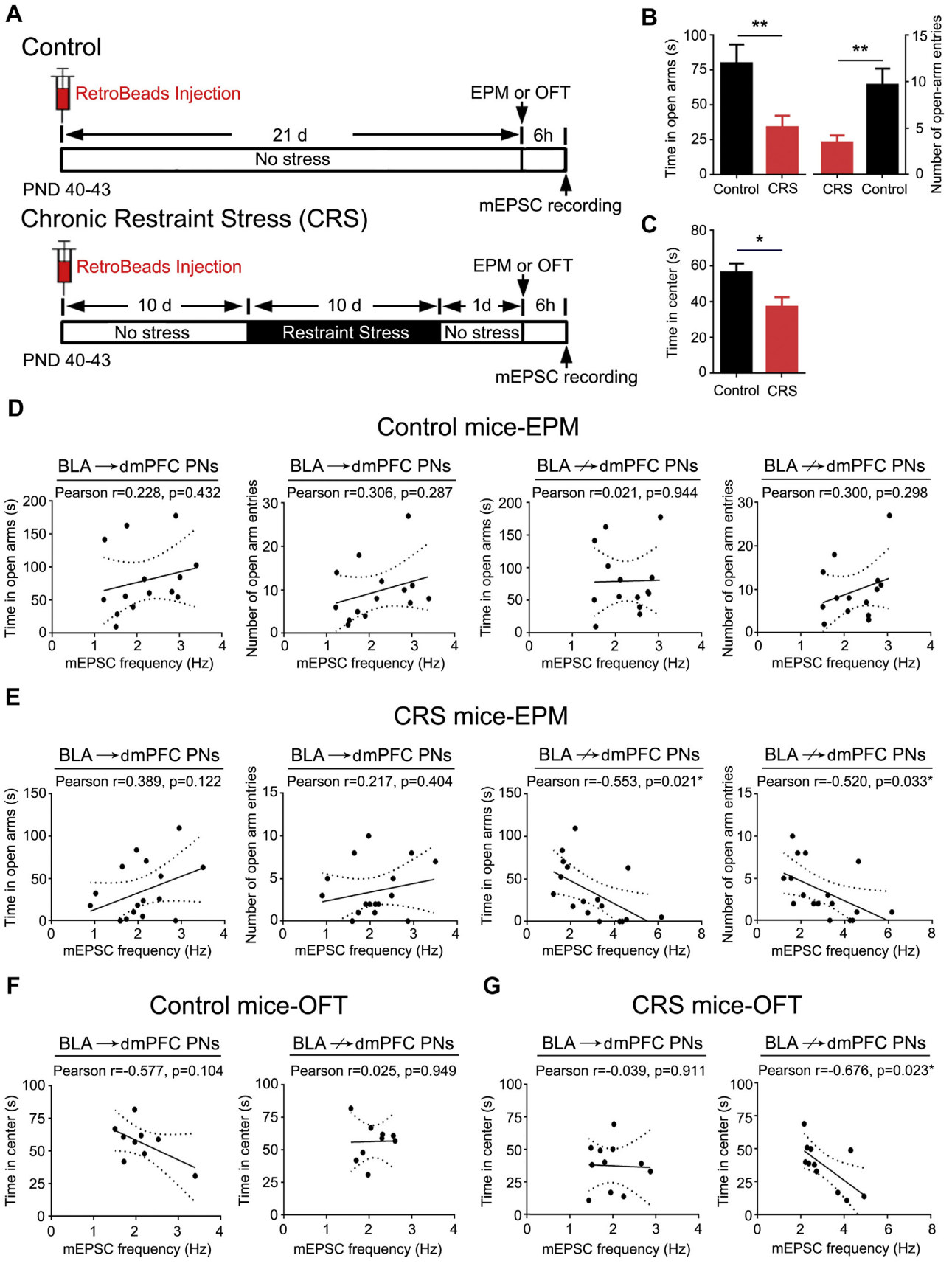
A
Control
RetroBeads Injection
EPM or OFT
21 d
6h
No stress
PND 40-43
mEPSC recording
Chronic Restraint Stress (CRS)
RetroBeads Injection
EPM or OFT
10 d
10 d
1d
6h
No stress
Restraint Stress
No stress
PND 40-43
mEPSC recording
B
Time in open arms (s)
Number of open-arm entries
Control
CRS
CRS
Control
C
Time in center (s)
Control
CRS
D
Control mice-EPM
BLA → dmPFC PNs
Pearson r=0.228, p=0.432
BLA → dmPFC PNs
Pearson r=0.306, p=0.287
BLA ↛ dmPFC PNs
Pearson r=0.021, p=0.944
BLA ↛ dmPFC PNs
Pearson r=0.300, p=0.298
Time in open arms (s)
Number of open arm entries
mEPSC frequency (Hz)
E
CRS mice-EPM
BLA → dmPFC PNs
Pearson r=0.389, p=0.122
BLA → dmPFC PNs
Pearson r=0.217, p=0.404
BLA ↛ dmPFC PNs
Pearson r=-0.553, p=0.021*
BLA ↛ dmPFC PNs
Pearson r=-0.520, p=0.033*
Time in open arms (s)
Number of open arm entries
mEPSC frequency (Hz)
F
Control mice-OFT
BLA → dmPFC PNs
Pearson r=-0.577, p=0.104
BLA ↛ dmPFC PNs
Pearson r=0.025, p=0.949
Time in center (s)
mEPSC frequency (Hz)
G
CRS mice-OFT
BLA → dmPFC PNs
Pearson r=-0.039, p=0.911
BLA ↛ dmPFC PNs
Pearson r=-0.676, p=0.023*
Time in center (s)
mEPSC frequency (Hz)

collateral colabeling (Figure 5A). Our first observation was that, in unstressed control mice, the spines in BLA→vHPC PNs had notably lower density but larger head size than the spines in the BLA→NAc PNs (Figure 5B–D). CRS significantly increased the spine density of BLA→vHPC PNs, relative to unstressed control mice, and this effect was absent in BLA→NAc PNs (Figure 5C). It also slightly but significantly increased the spine head size of BLA→vHPC PNs (Figure 5D). Furthermore, categorization of spine type revealed increased density in all three spine types in BLA→vHPC PNs after CRS (Figure 5E) and no effect in BLA→NAc PNs (Figure 5F). Finally, electrophysiological recordings indicated a significant CRS-related increase of mEPSC frequency, not amplitude, in BLA→vHPC, not BLA→NAc, PNs (Figure 5G, H), which was inversely correlated with exploration in the open arm in the elevated plus maze and center square in the open field test (Figure 5I–N). The increased glutamatergic afferents to BLA→vHPC PNs were absent in mice experiencing one session of acute restraint stress exposure (Supplemental Figure S5) but persisted after 1 week stress-free recovery from CRS (Supplemental Figure S6), indicating that it is a consequence of accumulative influence of prolonged stress exposure and lasts for long periods on stress removal. No changes in miniature inhibitory postsynaptic currents were observed in BLA→vHPC and BLA→NAc PNs following CRS (Supplemental Figure S7). Taken together, these data identify BLA PNs targeting the vHPC as at least one key output pathway that is functionally altered by CRS and linked to stress-induced increases in anxiety-like behavior (Figure 6).

DISCUSSION

The major finding of the current study was that chronic stress significantly altered the morphology and synaptic physiology of amygdala projection neurons in a manner that was selective to certain output pathways. Specifically, mice subjected to repeated restraint stress showed dendritic hypertrophy, spine enlargement, and increased synaptic glutamatergic transmission, but only in BLA PNs not projecting to the dmPFC. Subsequent experiments revealed that this same set of stress-related changes occurred in BLA PNs targeting the vHPC and not the NAc. Finally, greater stress-induced increases in synaptic transmission at BLA→vHPC PNs were found to correlate with higher levels of anxiety-like behavior.

Recent optogenetic studies have shown that photostimulating BLA PNs targeting the vHPC increases anxiety-like behavior and reduces social interaction, whereas photosilencing this pathway has the opposite effects, and, conversely, stimulating NAc-targeting BLA PNs promotes reward-seeking (20,22,23,39). The current findings that BLA→vHPC PNs are particularly susceptible to the effects of chronic stress and that functional alterations in these cells account for stress-induced anxiety-like behavior provide an important extension of these prior observations. Together, these findings identify the BLA→vHPC circuit as a critical locus regulating anxiety-like behavior and a principal site underlying stress-induced dysregulation of anxiety.

Neuronal and synaptic remodeling in BLA PNs, along with enhanced glutamatergic transmission, has been repeatedly associated with the negative consequence of stress (14,33,34,40), and prevention of these changes is paralleled by a protection against stress-induced increases in anxiety-like behavior (26,41). However, precisely how the BLA→vHPC circuit is functionally altered by stress to promote anxiety-like behavior remains to be determined. Increases in glutamatergic transmission coupled with the increased density of mature mushroom spines would be expected to result in stronger excitatory flow into this neuronal population after stress. These adaptations could increase responsiveness to external afferents in the face of functional competition among different neuronal populations within the BLA (21,42,43). In turn, this could potentially produce a bias in favor of a pro-anxiety BLA output pathway to produce the behavioral changes observed after stress. Notably, the density of immature thin and stubby spines was also increased in BLA→vHPC PNs, which might be associated with the generation of silent synapses following stress (15). One interesting avenue for future studies will be identifying the factors, such as molecular phenotype, that render this population particularly responsive to stress.

The observation that BLA PNs targeting the dmPFC did not exhibit increases in spine density and excitatory transmission after CRS echoes an earlier report that CRS led to hypotrophy in medial PFC (mPFC) PNs projecting to the entorhinal cortex, but not the BLA (44), and suggests that this pathway may be less susceptible to stress. In light of the posited role of the reciprocal BLA-mPFC circuit in stress coping (45,46), the retention of synaptic architecture and function in PNs interconnecting the regions may be of adaptive value. However, it is important to emphasize that this population was in fact not fully spared the effects of stress, and BLA→dmPFC PNs showed the same pronounced dendritic hypertrophy evident in the other BLA projection populations examined. It was surprising that dendritic hypertrophy was not associated with higher mEPSCs in this population, given that the overall number of spines would be expected to be higher even if density per dendritic segment was not. The absence of an increase in excitatory transmission is unlikely owing to reduced glutamate release probability onto BLA→dmPFC PNs because two measures indicating glutamate release probability, paired ratio of evoked EPSCs and the decay of *N*-methyl-D-aspartate receptor current by MK-801, were unaffected by stress. One possibility is that the generation of silent synapses

Figure 4. Excitatory transmission in basolateral amygdala (BLA) projection neurons (PNs) not targeting dorsomedial prefrontal cortex (BLA↛dmPFC) correlates with chronic restraint stress (CRS)–induced anxiety-like behavior. **(A)** Schematic of experimental designs. **(B)** Average time mice spent and entries into the open arms in the elevated plus maze (EPM). $n = 14$ control mice, $n = 17$ CRS-exposed mice. *t* test: $^{**}p < .01$. **(C)** Average time mice spent in the center square in the open field test (OFT). $n = 9$ control mice, $n = 11$ CRS-exposed mice. *t* test: $^{*}p < .05$. **(D)** Correlations between miniature excitatory postsynaptic current (mEPSC) frequency in BLA PNs targeting dmPFC (BLA→dmPFC) and BLA↛dmPFC and open arm exploration in unstressed control mice. **(E)** Correlations between mEPSC frequency in BLA→dmPFC and BLA↛dmPFC PNs and open arm exploration in CRS-exposed mice. **(F)** Correlations between mEPSC frequency in BLA→dmPFC and BLA↛dmPFC PNs and time in center square in unstressed control mice. **(G)** Correlations between mEPSC frequency in BLA→dmPFC and BLA↛dmPFC PNs and time in center square in CRS-exposed mice. Data are means ± SEM. PND, postnatal day.

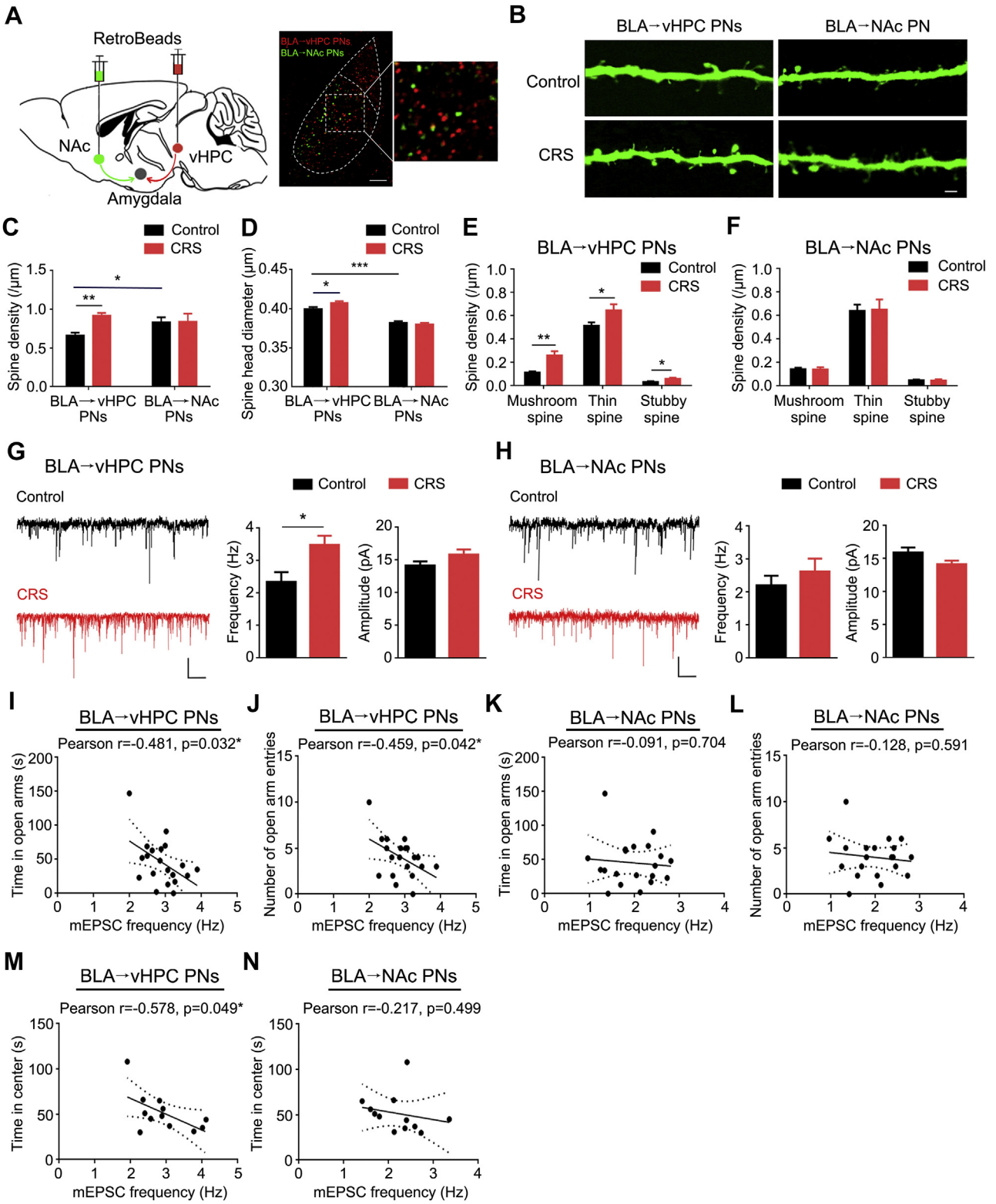

Figure 5. Chronic restraint stress (CRS) causes neuronal remodeling and increased excitatory transmission in basolateral amygdala (BLA) projection neurons (PNs) targeting ventral hippocampus (BLA→vHPC). **(A)** Schematic showing injection of red fluorescent RetroBeads into vHPC and green fluorescent RetroBeads in nucleus accumbens (NAc) and examples of labeled PNs in BLA. Very few PNs were colabeled (scale bar = 100 μm). **(B)** Examples of dendritic spines in BLA→vHPC and BLA→NAc PNs (scale bar = 2 μm). **(C)** Average spine density in BLA→vHPC and BLA→NAc PNs. PN group × CRS two-way

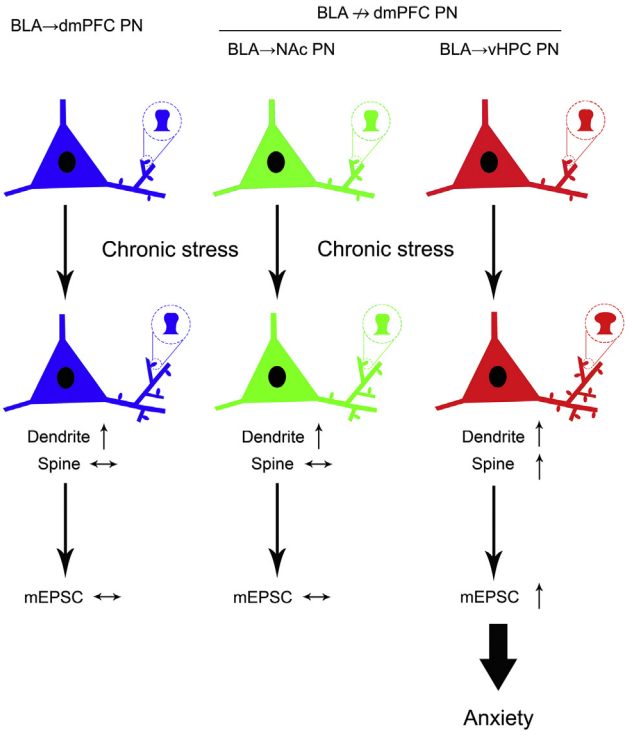

Figure 6. Summary schematic showing projection-specific remodeling of basolateral amygdala (BLA) projection neurons (PNs) after chronic stress. BLA PNs targeting dorsomedial prefrontal cortex (BLA→dmPFC) and a subset of those not targeting dmPFC (BLA↛dmPFC) projecting to the nucleus accumbens (NAc) show dendritic hypertrophy with no change in spine density or number of mushroom-type mature spines and no alteration in excitatory transmission. BLA→ventral hippocampus (vHPC) PNs exhibit dendritic hypertrophy, increased spine density, and a preponderance of mature spines. BLA→vHPC PNs also show augmented excitatory transmission, which correlates with stress-induced anxiety-like behavior. mEPSC, miniature excitatory postsynaptic current.

(15), which lack alpha-amino-3-hydroxy-5-methyl-4-isoxazole propionic acid receptors and alpha-amino-3-hydroxy-5-methyl-4-isoxazole propionic acid receptor–mediated glutamatergic transmission, could buffer an increase in excitatory transmission resulting from increased spine number.

Reciprocal connections between the BLA and mPFC are important for fear extinction, fear discrimination, and other processes requiring the resolution of conflicting information (47–50), and dendritic hypotrophy in mPFC neurons has been linked to stress and alcohol-related deficits in fear extinction (51,52). Moreover, optogenetic excitation of BLA→dmPFC PNs has been shown to increase conditioned fear after extinction (19). Thus, it remains possible that hypotrophy of BLA→dmPFC PNs might be associated with deficits in behaviors, such as fear extinction and discrimination, that were not examined in the current study. Another outstanding question is whether BLA PNs projecting to the ventromedial PFC are partially spared from the effects of chronic stress in the same way as BLA→dmPFC PNs, given that connections between the BLA and ventromedial PFC underlie inhibitory control of fear in extinction (19,50).

In recent years, it has become increasingly clear that the effect of stress on neuronal morphology and functions varies across brain regions (53–56). Chronic stress causes dendritic retraction in mPFC, dorsal hippocampus, and dorsomedial striatum but hypertrophy in the BLA, vHPC, orbitofrontal cortex, and dorsolateral striatum and no change in the lateral or central subnuclei of the amygdala (3,54,57–61). The findings of the current study, along with earlier work (44), show that the highly heterogeneous nature of stress effects extends to the level of specific output pathways within limbic structures. Taken together with advances in understanding of the epigenetic (57,58), genetic (59,60), and signaling (61,62) mechanisms underlying stress-related disturbances (63), these novel insights into the circuit-level effects of stress provide a foundation for modeling the pathophysiology of stress-related disease and improving their treatment.

ACKNOWLEDGMENTS AND DISCLOSURES

This work was supported by the National Basic Research Program of China (Grant No. 2014CB846100 [to B-XP]), National Natural Science Foundation of China (Grant Nos. 91332123 [to B-XP], 81601179 [to B-XP], 81503079 [to J-YZ], 81741759 [to B-XP], and 31700916 [principal investigator, Zhi-Peng Liu]), Natural Science Foundation of Jiangxi Province (Grant Nos. 20143ACB21002 [to B-XP], 20172BCB22005 [to B-XP], KJLD14013 [to B-XP], and 20161BAB215204 [to J-YZ]), and National Institute on Alcohol Abuse and Alcoholism Intramural Research Program (to AH).

The authors report no biomedical financial interests or potential conflicts of interest.

ARTICLE INFORMATION

From the Laboratory of Fear and Anxiety Disorders (J-YZ, T-HL, YH, H-QP, W-HZ, B-ML, B-XP), Institute of Life Science, Department of Neurology (J-YZ, X-PY, B-XP), the 2nd Affiliated Hospital, and Human Aging Research Institute (X-LT, B-XP), School of Life Science, Nanchang University, Nanchang; Department of Neurobiology (X-DW), Key Laboratory of Medical

analysis of variance (ANOVA): interaction ($F_{1,26}$ = 2.75, p = .109), main effect of PN group ($F_{1,26}$ = 0.37, p = .54), main effect of CRS ($F_{1,26}$ = 3.05, p = .093). For BLA→vHPC PNs, n = 7 neurons/4 control mice, n = 8 neurons/4 CRS-exposed mice. For BLA→NAc PNs, n = 7 neurons/6 control mice, n = 9 neurons/7 CRS-exposed mice. **(D)** Average spine head diameter in BLA→vHPC and BLA→NAc PNs. PN group × CRS two-way ANOVA: interaction ($F_{1,16198}$ = 4.64, p = .03), main effect of PN group ($F_{1,16198}$ = 95.13, p < .001), main effect of CRS ($F_{1,16198}$ = 1.51, p = .218). For BLA→vHPC PNs, n = 2165 spines/7 control neurons, n = 4914 spines/8 CRS neurons. For BLA→NAc PNs, n = 3966 spines/7 control neurons, n = 5157 spines/9 CRS neurons. **(E, F)** Average density in mushroom, thin, and stubby spines in BLA→vHPC **(E)** and BLA→NAc **(F)** PNs. For BLA→vHPC PNs, spine type × CRS two-way ANOVA: interaction ($F_{2,36}$ = 2.55, p = .092), main effect of spine type ($F_{2,36}$ = 183.4, p < .001), main effect of CRS ($F_{1,36}$ = 18.55, p < .001). t test: *p < .05, **p < .01. For BLA→NAc PNs, spine type × CRS two-way ANOVA: interaction ($F_{2,36}$ = 0.01, p = .988), main effect of spine type ($F_{2,42}$ = 99.61, p < .001), main effect of CRS ($F_{1,42}$ = 0.003, p = .953). **(G, H)** Example traces and average miniature excitatory postsynaptic current (mEPSC) frequency and amplitude in BLA→vHPC **(G)** and BLA→NAc **(H)** PNs. For BLA→vHPC PNs, n = 10 neurons/5 control mice, n = 13 neurons/5 CRS-exposed mice. For BLA→NAc PNs, n = 10 neurons/4 control mice, n = 14 neurons/5 CRS-exposed mice. t test: *p < .05 (scale bar = 1 second, 10 picoamperes). **(I, J)** Correlations between mEPSC frequency in BLA→vHPC PNs and open arm exploration in elevated plus maze in CRS-exposed mice. **(K, L)** Correlations between mEPSC frequency in BLA→NAc PNs and open arm exploration in elevated plus maze in CRS-exposed mice. **(M, N)** Correlations between mEPSC frequency in BLA→vHPC **(M)** and BLA→vHPC **(N)** PNs and time in center square in open field test in CRS-exposed mice. Data are means ± SEM.

Neurobiology of Ministry of Health of China and Zhejiang Provincial Key Laboratory of Neurobiology, Zhejiang University School of Medicine, Hangzhou; Shanghai Mental Health Center (T-FY), Shanghai Jiaotong University School of Medicine, Shanghai, China; and Laboratory of Behavioral and Genomic Neuroscience (AH), National Institute on Alcohol Abuse and Alcoholism, National Institutes of Health, Bethesda, Maryland.

J-YZ and T-HL contributed equally to this work.

Address correspondence to Bing-Xing Pan, Ph.D., M.D., Laboratory of Fear and Anxiety Disorders, Institute of Life Science, XueFu Road 999, HongGuTan New Area, Nanchang, Jiangxi 330031, China; E-mail: panbingxing@ncu.edu.cn.

Received Feb 14, 2018; revised Jun 20, 2018; accepted Jun 22, 2018.

Supplementary material cited in this article is available online at https://doi.org/10.1016/j.biopsych.2018.06.019.

REFERENCES

1. McEwen BS, Morrison JH (2013): The brain on stress: Vulnerability and plasticity of the prefrontal cortex over the life course. Neuron 79:16–29.
2. McEwen BS, Bowles NP, Gray JD, Hill MN, Hunter RG, Karatsoreos IN, *et al.* (2015): Mechanisms of stress in the brain. Nat Neurosci 18:1353–1363.
3. Dias-Ferreira E, Sousa JC, Melo I, Morgado P, Mesquita AR, Cerqueira JJ, *et al.* (2009): Chronic stress causes frontostriatal reorganization and affects decision-making. Science 325(5940):621–625.
4. de Kloet ER, Joels M, Holsboer F (2005): Stress and the brain: From adaptation to disease. Nat Rev Neurosci 6:463–475.
5. Luthi A, Luscher C (2014): Pathological circuit function underlying addiction and anxiety disorders. Nat Neurosci 17:1635–1643.
6. Chattarji S, Tomar A, Suvrathan A, Ghosh S, Rahman MM (2015): Neighborhood matters: Divergent patterns of stress-induced plasticity across the brain. Nat Neurosci 18:1364–1375.
7. Davis M, Walker DL, Miles L, Grillon C (2010): Phasic vs sustained fear in rats and humans: Role of the extended amygdala in fear vs anxiety. Neuropsychopharmacology 35:105–135.
8. Etkin A, Wager TD (2007): Functional neuroimaging of anxiety: A meta-analysis of emotional processing in PTSD, social anxiety disorder, and specific phobia. Am J Psychiatry 164:1476–1488.
9. Roozendaal B, McEwen BS, Chattarji S (2009): Stress, memory and the amygdala. Nat Rev Neurosci 10:423–433.
10. Rauch SL, Whalen PJ, Shin LM, McInerney SC, Macklin ML, Lasko NB, *et al.* (2000): Exaggerated amygdala response to masked facial stimuli in posttraumatic stress disorder: A functional MRI study. Biol Psychiatry 47:769–776.
11. Maroun M, Pericles JI, Krista LB, Alexandra K, Andrew H, Cara LW, *et al.* (2013): Fear extinction deficits following acute stress associate with increased spine density and dendritic retraction in basolateral amygdala neurons. Eur J Neurosci 38:2611–2620.
12. Mozhui K, Karlsson RM, Kash TL, Ihne J, Norcross M, Patel S, *et al.* (2010): Strain differences in stress responsivity are associated with divergent amygdala gene expression and glutamate-mediated neuronal excitability. J Neurosci 30:5357–5367.
13. Holmes A, Wellman CL (2009): Stress-induced prefrontal reorganization and executive dysfunction in rodents. Neurosci Biobehav Rev 33:773–783.
14. Vyas A, Mitra R, Shankaranarayana Rao BS, Chattarji S (2002): Chronic stress induces contrasting patterns of dendritic remodeling in hippocampal and amygdaloid neurons. J Neurosci 22:6810–6818.
15. Suvrathan A, Bennur S, Ghosh S, Tomar A, Anilkumar S, Chattarji S (2014): Stress enhances fear by forming new synapses with greater capacity for long-term potentiation in the amygdala. Philos Trans R Soc Lond B Biol Sci 369:20130151.
16. LeDoux J (2007): The amygdala. Curr Biol 17:R868–R874.
17. Beyeler A, Namburi P, Glober GF, Simonnet C, Calhoon GG, Conyers GF, *et al.* (2016): Divergent routing of positive and negative information from the amygdala during memory retrieval. Neuron 90:348–361.
18. Grundemann J, Luthi A (2015): Ensemble coding in amygdala circuits for associative learning. Curr Opin Neurobiol 35:200–206.
19. Senn V, Wolff SB, Herry C, Grenier F, Ehrlich I, Gründemann J, *et al.* (2014): Long-range connectivity defines behavioral specificity of amygdala neurons. Neuron 81:428–437.
20. Namburi P, Beyeler A, Yorozu S, Calhoon G, Halbert SA, Wichmann R, *et al.* (2015): A circuit mechanism for differentiating positive and negative associations. Nature 520:675–678.
21. Kim J, Pignatelli M, Xu S, Itohara S, Tonegawa S (2016): Antagonistic negative and positive neurons of the basolateral amygdala. Nat Neurosci 19:1636–1646.
22. Felix-Ortiz AC, Beyeler A, Seo C, Leppla CA, Wildes CP, Tye KM, *et al.* (2013): BLA to vHPC inputs modulate anxiety-related behaviors. Neuron 79:658–664.
23. Stuber GD, Sparta DR, Stamatakis AM, van Leeuwen WA, Hardjoprajitno JE, Cho S, *et al.* (2011): Excitatory transmission from the amygdala to nucleus accumbens facilitates reward seeking. Nature 475:377–380.
24. Liu ZP, Song C, Wang M, He Y, Xu XB, Pan HQ, *et al.* (2014): Chronic stress impairs GABAergic control of amygdala through suppressing the tonic GABAA receptor currents. Mol Brain 7:32.
25. Gourley SL, Swanson AM, Koleske AJ (2013): Corticosteroid-induced neural remodeling predicts behavioral vulnerability and resilience. J Neurosci 33:3107–3112.
26. Mitra R, Adamec R, Sapolsky R (2009): Resilience against predator stress and dendritic morphology of amygdala neurons. Behav Brain Res 205:535–543.
27. Smith DL, Pozueta J, Gong B, Arancio O, Shelanski M (2009): Reversal of long-term dendritic spine alterations in Alzheimer disease models. Proc Natl Acad Sci U S A 106:16877–16882.
28. Cahill ME, Bagot RC, Gancarz AM, Walker DM, Sun H, Wang ZJ, *et al.* (2016): Bidirectional synaptic structural plasticity after chronic cocaine administration occurs through Rap1 small GTPase signaling. Neuron 89:566–582.
29. Sylvie R, Ronald O, Djamel AA, Hank FK, Pierre B, Monica M, *et al.* (1998): Serotonin receptor 1A knockout: An animal model of anxiety-related disorder. Proc Natl Acad Sci U S A 95:14476–14481.
30. Berry KP, Nedivi E (2017): Spine dynamics: Are they all the same? Neuron 96:43–55.
31. Bhatt DH, Zhang S, Gan WB (2009): Dendritic spine dynamics. Annu Rev Physiol 71:261–282.
32. Segal M (2005): Dendritic spines and long-term plasticity. Nat Rev Neurosci 6:277–284.
33. Adamec R, Hebert M, Blundell J, Mervis RF (2012): Dendritic morphology of amygdala and hippocampal neurons in more and less predator stress responsive rats and more and less spontaneously anxious handled controls. Behav Brain Res 226:133–146.
34. Vyas A, Pillai AG, Chattarji S (2004): Recovery after chronic stress fails to reverse amygdaloid neuronal hypertrophy and enhanced anxiety-like behavior. Neuroscience 128:667–673.
35. Qiao H, Li MX, Xu C, Chen HB, An SC, Ma XM, *et al.* (2016): Dendritic spines in depression: What we learned from animal models. Neural Plast 2016:8056370.
36. Masneuf S, Gionta EL, Colacicco G, Pleil KE, Li C, Crowley N, *et al.* (2014): Glutamatergic mechanisms associated with stress-induced amygdala excitability and anxiety-related behavior. Neuropharmacology 85:190–197.
37. Wellman CL, Izquierdo A, Garrett JE, Martin KP, Carroll J, Millstein R, *et al.* (2007): Impaired stress-coping and fear extinction and abnormal corticolimbic morphology in serotonin transporter knock-out mice. J Neurosci 27:684–691.
38. Bannerman DM, Sprengel R, Sanderson DJ, McHugh SB, Rawlins JNP, Monyer H, *et al.* (2014): Hippocampal synaptic plasticity, spatial memory and anxiety. Nat Rev Neurosci 15:181–192.
39. Felix-Ortiz AC, Tye KM (2014): Amygdala inputs to the ventral hippocampus bidirectionally modulate social behavior. J Neurosci 34:586–595.
40. Mitra R, Sapolsky RM (2008): Acute corticosterone treatment is sufficient to induce anxiety and amygdaloid dendritic hypertrophy. Proc Natl Acad Sci U S A 105:5573–5578.
41. Mitra R, Ferguson D, Sapolsky RM (2009): SK2 potassium channel overexpression in basolateral amygdala reduces anxiety, stress-induced corticosterone secretion and dendritic arborization. Mol Psychiatry 14:847–855.

42. Han JH, Kushner SA, Yiu AP, Cole CJ, Matynia A, Brown RA, *et al.* (2007): Neuronal competition and selection during memory formation. Science 316:457–460.
43. Lee SC, Amir A, Haufler D, Pare D (2017): Differential recruitment of competing valence-related amygdala networks during anxiety. Neuron 96:81–88.
44. Shansky RM, Hamo C, Hof PR, McEwen BS, Morrison JH (2009): Stress-induced dendritic remodeling in the prefrontal cortex is circuit specific. Cereb Cortex 19:2479–2484.
45. Keding TJ, Herringa RJ (2016): Paradoxical prefrontal-amygdala recruitment to angry and happy expressions in pediatric post-traumatic stress disorder. Neuropsychopharmacology 41:2903–2912.
46. Wolf RC, Herringa RJ (2016): Prefrontal-amygdala dysregulation to threat in pediatric posttraumatic stress disorder. Neuropsychopharmacology 41:822–831.
47. Burgos-Robles A, Burgos-Robles A, Kimchi EY, Izadmehr EM, Porzenheim MJ, Ramos-Guasp WA, *et al.* (2017): Amygdala inputs to prefrontal cortex guide behavior amid conflicting cues of reward and punishment. Nat Neurosci 20:824–835.
48. Banks SJ, Eddy KT, Angstadt M, Nathan PJ, Phan KL (2007): Amygdala-frontal connectivity during emotion regulation. Soc Cogn Affect Neurosci 2:303–312.
49. Likhtik E, Pelletier JG, Paz R, Pare D (2005): Prefrontal control of the amygdala. J Neurosci 25:7429–7437.
50. Bukalo O, Pinard CR, Silverstein S, Brehm C, Hartley ND, Whittle N, *et al.* (2015): Prefrontal inputs to the amygdala instruct fear extinction memory formation [published online ahead of print Jul 31]. Sci Adv.
51. Izquierdo A, Wellman CL, Holmes A (2006): Brief uncontrollable stress causes dendritic retraction in infralimbic cortex and resistance to fear extinction in mice. J Neurosci 26:5733–5738.
52. Holmes A, Fitzgerald PJ, MacPherson KP, DeBrouse L, Colacicco G, Flynn SM, *et al.* (2012): Chronic alcohol remodels prefrontal neurons and disrupts NMDAR-mediated fear extinction encoding. Nat Neurosci 15:1359–1361.
53. Sousa N, Almeida OF (2012): Disconnection and reconnection: The morphological basis of (mal)adaptation to stress. Trends Neurosci 35:742–751.
54. Liston C, Miller MM, Goldwater DS, Radley JJ, Rocher AB, Hof PR, *et al.* (2006): Stress-induced alterations in prefrontal cortical dendritic morphology predict selective impairments in perceptual attentional set-shifting. J Neurosci 26:7870–7874.
55. Sheline YI, Wang PW, Gado MH, Csernansky JG, Vannier MW (1996): Hippocampal atrophy in recurrent major depression. Proc Natl Acad Sci U S A 93:3908–3913.
56. McEwen BS, Nasca C, Gray JD (2016): Stress effects on neuronal structure: Hippocampus, amygdala, and prefrontal cortex. Neuropsychopharmacology 41:3–23.
57. McEwen BS (2017): Allostasis and the epigenetics of brain and body health over the life course: The brain on stress. JAMA Psychiatry 74:551–552.
58. Turecki G, Meaney MJ (2016): Effects of the social environment and stress on glucocorticoid receptor gene methylation: A systematic review. Biol Psychiatry 79:87–96.
59. Bennett MR, Lagopoulos J (2014): Stress and trauma: BDNF control of dendritic-spine formation and regression. Prog Neurobiol 112:80–99.
60. Issler O, Haramati S, Paul ED, Maeno H, Navon I, Zwang R, *et al.* (2014): MicroRNA 135 is essential for chronic stress resiliency, antidepressant efficacy, and intact serotonergic activity. Neuron 83:344–360.
61. Myers B, McKlveen JM, Herman JP (2014): Glucocorticoid actions on synapses, circuits, and behavior: implications for the energetics of stress. Front Neuroendocrinol 35:180–196.
62. Qin Z, Zhou X, Pandey NR, Vecchiarelli HA, Stewart CA, Zhang X, *et al.* (2015): Chronic stress induces anxiety via an amygdalar intracellular cascade that impairs endocannabinoid signaling. Neuron 85:1319–1331.
63. Hariri AR, Holmes A (2015): Finding translation in stress research. Nat Neurosci 18:1347–1352.